Photoluminescence of green InGaN/GaN MQWs grown on pre-wells*

Shou-Qiang Lai(赖寿强)[1], Qing-Xuan Li(李青璇)[1], Hao Long(龙浩)[1], Jin-Zhao Wu(吴瑾照)[1], Lei-Ying Ying(应磊莹)[1], Zhi-Wei Zheng(郑志威)[1], Zhi-Ren Qiu(丘志仁)[2], and Bao-Ping Zhang(张保平)[1,†]

[1] *School of Electronic Science and Engineering, Xiamen University, Xiamen* 361005, *China*
[2] *State Key Laboratory of Optoelectronic Materials and Technologies, Sun Yat-sen University, Guangzhou* 510275, *China*

(Received 30 April 2020; revised manuscript received 10 August 2020; accepted manuscript online 9 September 2020)

Photoluminescence (PL) characteristics of the structure consisting of green InGaN/GaN multiple quantum wells (MQWs) and low indium content InGaN/GaN pre-wells are investigated. Several PL peaks from pre-wells and green InGaN/GaN MQWs are observed. The peak energy values for both pre-wells and green InGaN/GaN MQWs display an S-shaped variation with temperature. In addition, the differences in the carrier localization effect, defect density, and phonon–exciton interaction between the pre-wells and green InGaN/GaN MQWs, and the internal quantum efficiency of the sample are studied. The obtained results elucidate the mechanism of the luminescence characteristics of the sample and demonstrate the significant stress blocking effect of pre-wells.

Keywords: InGaN/GaN, photoluminescence, pre-wells, green LED

PACS: 78.66.Fd, 78.67.De, 85.60.Jb **DOI:** 10.1088/1674-1056/abb65b

1. Introduction

Group III-nitrides (InN, GaN, AlN, and their alloys) are direct-gap semiconductor materials with tunable direct bandgaps ranging from the visible to the ultraviolet region of the electromagnetic spectrum. Among these materials, InGaN is a core material for visible light-emitting devices (LEDs) and AlGaN is a key material for deep-ultraviolet optoelectronic devices.[1] With the development of crystal growth technology, blue and green LEDs and laser diodes have been used commercially in many fields such as full-color display, optical storage, and solid-state lighting.[2,3] For the well-known "green gap",[4] the luminous efficiency of green InGaN/GaN MQWs grown on GaN is generally below the luminous efficiency of blue LEDs due to the large lattice mismatch between GaN and InGaN with high indium content, which leads the crystal quality to severely decline and generates a large number of non-radiative recombination centers (NRCs).[5] Therefore, improving the luminous efficiency of green InGaN/GaN multiple quantum wells (MQWs) is highly desirable.[6,7] In recent years, several methods such as changing the substrate,[8] controlling the curvature of the InGaN layers[9,10] and inserting a prestrained film before InGaN/GaN MQWs have been reported to improve the properties of green InGaN/GaN MQWs.[11–14] Langer *et al.*[15] have reported that a full or partial relaxation of InGaN may be vital for eliminating the "green gap"; for this approach, the technique of growing green InGaN/GaN MQWs on pre-wells rather than on GaN has attracted great interest because of the smaller lattice mismatch of such structures and the advanced techniques available for the growth of low indium content pre-wells. Thus, the studies of high indium content InGaN/GaN MQWs grown on pre-wells are important because of their practical value for improving the properties of green InGaN/GaN MQWs.[16–20] Despite the many advantages of the above-described approach, several challenges still must be overcome in order to eliminate the "green gap". In particular, the stress in green InGaN/GaN MQWs can be relaxed because of the insertion of pre-wells, and therefore, further studies are necessary to reveal the specific carrier recombination mechanism and stress blocking effect of pre-wells and to compare the photoluminescence characteristics of the peaks at different wavelengths.

In this work, the temperature-dependent photoluminescence (TDPL) method and the time-resolved photoluminescence (TRPL) method are used to study the optical properties of green InGaN/GaN MQWs with low indium content pre-wells. Using TDPL measurements, we analyze the differences in the defect density and phonon–exciton interaction strength between peaks. Additionally, the internal quantum efficiency of the sample is obtained from the TRPL experiments. These results elucidate the mechanism of the special photoluminescence characteristics of green MQWs grown on pre-wells and demonstrate the advantages of green MQWs grown on pre-wells.

*Project supported by the Science Challenge Project, China (Grant No. TZ2016003), the National Key Research and Development Program of China (Grant Nos. 2016YFB0400803 and 2017YFE0131500), and the Fund from the State Key Laboratory of Optoelectronic Materials and Technologies, Sun Yat-sen University, China.

†Corresponding author. E-mail: bzhang@xmu.edu.cn

2. Sample structure and experiment

Figure 1 shows the structure of the sample. The width of well structure exceeding 4 nm usually results in a stronger polarization effect between the well and the barrier, reducing the internal quantum efficiency (IQE) of the LED. Thus, the well width of the LED is mostly limited to a value below 3.5 nm.[21] In this work, the sample was designed to contain two different parts: the pre-well that is comprised of 5 periods of 1.5-nm $In_{0.05}Ga_{0.95}N$ quantum wells and 2-nm GaN barriers, and the green MQW that is composed of 10 periods of 3-nm $In_{0.25}Ga_{0.75}N$ quantum wells and 12-nm GaN barriers.

The sample was mounted in a closed-cycle He-cryostat and the temperature was varied from 17 K to 300 K. A 325-nm CW He–Cd laser with the excitation power of 0.32 mW was used as an excitation source. The PL signal from the sample was dispersed by a Princeton instruments ACTON-Spectrapro-3000i monochromator and was detected by a thermoelectrical-cooled Synapse CCD detector. The sample was excited by an Nd:YAG mode-locked laser with frequency doubling to 375 nm, and the pulse width was adjusted to 25 ps and the repetition frequency was modulated to 10 Hz. The steady-state spectra were collected by using a JOBIN YVON Trax 550 spectrometer with a resolution of 0.02 nm. The transient spectrum was collected and recorded by using a streak camera and a CCD recorder, finally, the TRPL signal from the sample was obtained.

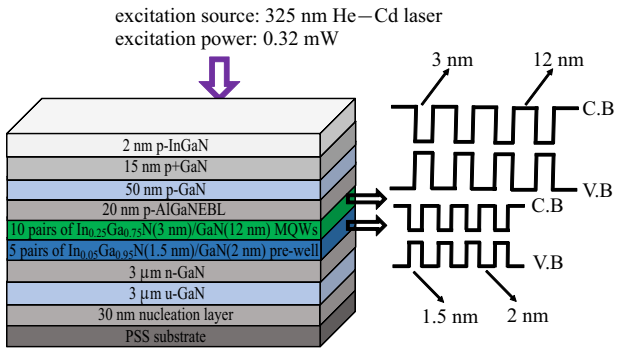

Fig. 1. Schematic diagram of green InGaN/GaN MQWs with low indium content InGaN/GaN pre-wells.

3. Experimental results and analyses

During epitaxial growth of InGaN, especially when the GaN underlayer is very thick, the stress caused by lattice mismatch can be concentrated in InGaN. Therefore, when the indium content is large, a large stress is caused, thus defects are easily formed, resulting in a reduction in luminous efficiency of green MQW. The stress caused by the lattice mismatch can be expressed as[22]

$$\varepsilon_{\parallel} = \frac{a_{\mathrm{s}} - a_{\mathrm{f}}}{a_{\mathrm{f}}}, \tag{1}$$

$$\varepsilon_{\perp} = -2 \cdot \nu \cdot \frac{a_{\mathrm{s}} - a_{\mathrm{f}}}{a_{\mathrm{f}}}, \tag{2}$$

where $\varepsilon_{\parallel}$ and $\varepsilon_{\perp}$ are the strain components parallel and perpendicular to the growing plane, respectively. In our case, a_{f} and a_{s} represent the in-plane lattice constant of $In_{0.25}Ga_{0.75}N$ and the film beneath the green MQWs, respectively. Lattice constant and ν (Poisson's ratio) of $In_xGa_{1-x}N$ can be obtained according to the Vegard rule and are shown in Table 1. These lattice constant values are then used to obtain the misfit strain values according to Eq. (1). Specifically, the misfit between pre-well and green MQW is 2.16%, much smaller than the misfit of 2.70% between GaN and green MQW. Thus, the insertion of pre-wells effectively reduces the epitaxial stress in green MQWs.

Table 1. Parameters of InN, GaN, and $In_xGa_{1-x}N$.

Parameters	GaN	InN	$In_{0.05}Ga_{0.95}N$	$In_{0.25}Ga_{0.75}N$
a/nm	0.3189	0.3543	0.32067	0.32775
ν	0.183	0.272	0.18745	0.20525

Additionally, when green MQWs are grown on pre-wells, lattice constants of InGaN in pre-wells and green MQWs are both larger than that of GaN, forming a tensile stress to the GaN interlayer locating between the pre-well and green wells. As a result, the tensile stress will enlarge the in-plane lattice constant of this GaN interlayer. In other words, part of the stress in green InGaN will be absorbed by the interlayer, thus reducing the effect of the stress in green InGaN. For the low indium content of pre-wells and the thin GaN interlayer, it is reasonable to expect that the stress from the green InGaN may affect the InGaN in pre-wells, resulting in a large stress and acoustic phonon interaction in the pre-wells.

Figure 2 shows the PL spectra at a temperature of 85 K. The fitting identifies four peaks which we denoted as peaks 1–4, with the peak energy values of 2.29, 2.35, 2.83 and 2.95 eV, respectively. Peaks 1 and 2 originate from $In_{0.25}Ga_{0.75}N$ (3 nm)/GaN (12 nm) MQWs and peak 3 sources from $In_{0.05}Ga_{0.95}N$ (1.5 nm)/GaN (2 nm) pre-wells while peak 4 arises from the donor–acceptor pair recombination in p-GaN.[23–25]

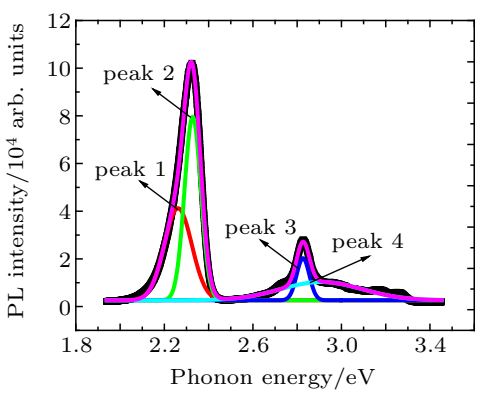

Fig. 2. PL spectra varying with photon energy at low temperature (85 K).

For the normalized PL spectra at different temperatures shown in Fig. 3, a long wavelength shoulder can be observed at 2.25 eV (550 nm); this shoulder is derived from the bound state in green InGaN/GaN MQWs.

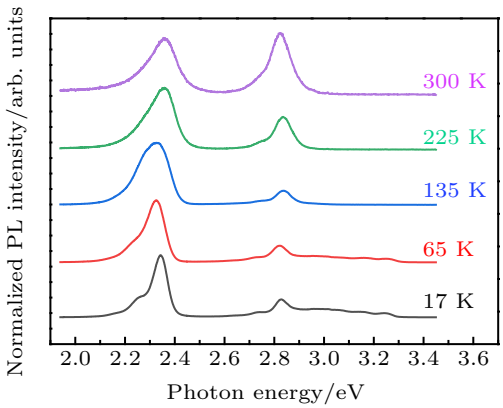

Fig. 3. Normalized PL spectra varying with photon energy at different temperatures.

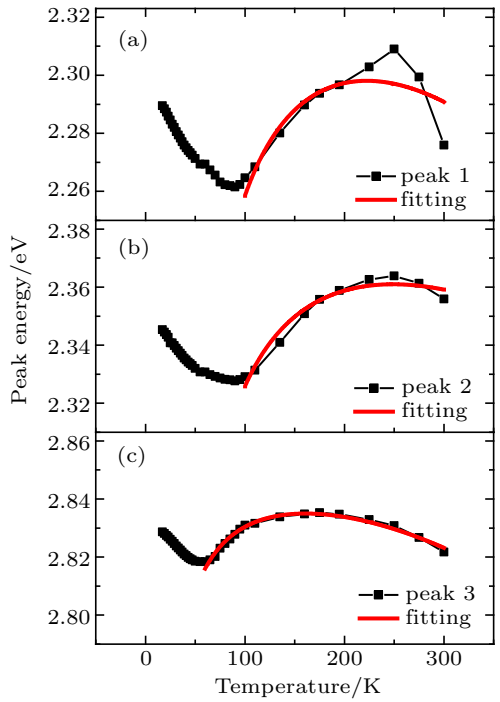

Fig. 4. Temperature-dependent PL peak energy obtained from Varshini fitting separately for (a) peak 1, (b) peak 2, and (c) peak 3.

The energy values of peaks 1–3 at different temperatures are shown in Fig. 4. It is clear from Fig. 4 that with the increase of temperature, the ratio between the PL intensities of pre-wells and green InGaN/GaN MQWs increases continuously, indicating that there are more NRCs in green InGaN/GaN MQWs. In the InGaN/GaN MQWs, the fluctuation of indium content and phase separation will induce the indium to cluster, forming localization potential dips. An examination of Fig. 4 also clearly shows that the energy values of peaks 1–3 exhibit an obvious S-shaped behavior (red-blue-red) with the increase of temperature, demonstrating the localization effect in the InGaN materials.[26,27] Additionally, the peak energy of low indium content pre-wells begins to blue-shift at a lower temperature because of their more shallow localized states. The temperature dependence of the bandgap energy can be described by the Varshini formula as follows:[28–30]

$$E_{\rm g}(T) = E_0 - \frac{\alpha \times T^2}{(\beta + T)} - \frac{\sigma^2}{k_{\rm B} \times T}, \tag{3}$$

where E_0 is the bandgap energy at 0 K (subscript 0 denotes the temperature of 0 K), T is the temperature in Kelvin, α and β are the parameters of the Varshini fitting, σ indicates the degree of the localization effect, and $k_{\rm B}$ is the Boltzmann constant.[31] The fitting results for different peaks are shown in Fig. 4 and the parameters obtained from Varshini fitting are shown in Table 2. The values of σ for peaks 1–3 are 30.4, 26.6, and 14.6 meV, respectively.

Table 2. Parameters obtained from modified band-tail model.

	Peak 1	Peak 2	Peak 3
E_0/eV	2.37	2.41	2.86
α/(meV/K)	25.1	13.18	10.9
β/K	5.18×10^4	4.96×10^4	3.71×10^4
σ/meV	30.4	26.6	14.6

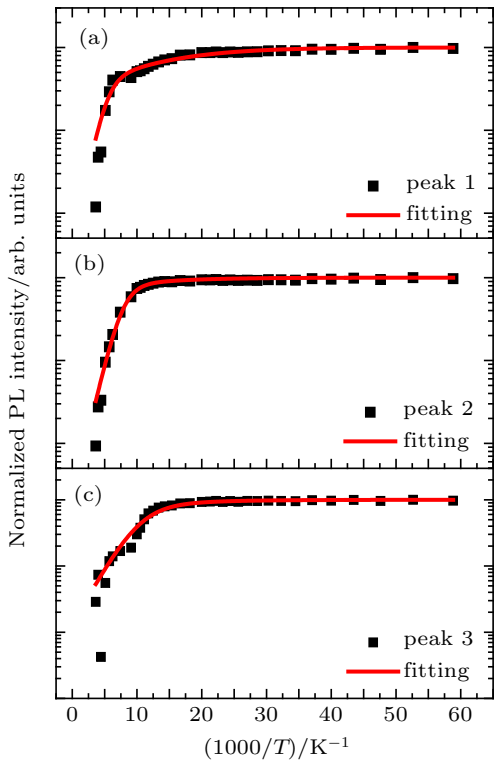

Fig. 5. Arrhenius plots of normalized PL intensity *versus* temperature of (a) peak 1, (b) peak 2, and (c) peak 3, respectively.

To study the properties of the localization centers and the defect density, a two-channel Arrhenius model[11] is used to analyze the temperature dependence of the PL intensity

$$I(T) = \frac{I_0}{\left[1 + A_1 \cdot \exp\left(-\frac{E_{\rm a1}}{k_{\rm B} \cdot T}\right) + A_2 \cdot \exp\left(-\frac{E_{\rm a2}}{k_{\rm B} \cdot T}\right)\right]}, \tag{4}$$

where I_0 is the integrated PL intensity at low temperature which is 17 K in our study, A_1 is the constant related to the density of the localization states, E_{a1} is the localization energy of the bound-exciton, A_2 is related to the defect density, E_{a2} is the activation energy of the corresponding nonradiative process, and k_B is the Boltzmann constant. Figure 5 shows the fitting results obtained from this model, and Table 3 presents the parameters obtained from the fitting.

Table 3. Parameters obtained from two-channel Arrhenius model.

	Peak 1	Peak 2	Peak 3
A_1	249.8	476.4	75.4
A_2	2.47	0.67	0.80
E_{a1}/meV	76.7	66.4	35.1
E_{a2}/meV	10.1	11.2	10.2

At low temperature, the carriers are strongly trapped in the localized states, and the non-radiative recombination process is frozen and inactive. By contrast, at higher temperatures the carriers trapped in localized states can overcome the localization barrier, leading to the phenomenon of "thermal escape of carriers", and the escaped carriers can be trapped by non-radiative centers. Additionally, the non-radiative recombination process is activated, leading to the PL intensity to decay. The above-described results can be summarized as follows. (i) The E_{a1} value for the peak from green InGaN/GaN MQW is larger than the E_{a1} for the peak from the pre-well, suggesting that the former has larger localization potential barrier because of their larger indium content. It is noteworthy that peak 1 corresponds to the localized state induced by the component with the highest indium content, and thus has the largest localization potential barrier. The fitting results are consistent with the results of Varshini fitting. (ii) The value of A_1 for peak 2 is larger than that for peak 1, suggesting that the density of localized states is higher for peak 2, or in other words, that the stress in most of the green MQWs is relaxed. (iii) The E_{a2} values of the pre-wells and green InGaN/GaN MQWs are almost the same, suggesting that similar defect states exist in both pre-wells and green InGaN/GaN MQWs; however, the A_2 value for peak 1 is larger than that for peak 2, suggesting that the defect density around the deep localized states is higher due to the existence of larger stress. We note that the defect density in green InGaN/GaN MQWs (A_2, 0.67) is even smaller than that in pre-wells (A_2, 0.80), indicating that to a great extent, the stress in corresponding green InGaN/GaN MQWs is relaxed.[11]

Figure 6 shows the temperature dependence of linewidth of each peak. With the increase of temperature, the linewidth of peak 1 first decreases slightly, then gradually increases; on the other hand, peak 2 and peak 3 both follow an obvious W-shaped (decrease-increase-decrease-increase) temperature dependence. However, as shown in Fig. 4, all the peaks follow the well-known S-shaped (decrease-increase-decrease) temperature dependence in the peak energy. Therefore, the temperature dependence of the emission peak is somewhat complicated. According to Wang *et al.*,[30] the temperature dependence of luminescence characteristics is strongly dependent on the carrier concentration: at low carrier concentration, the peak energy exhibits an S-shaped temperature dependence of peak energy, while the linewidth follows a W-shaped temperature dependence; at medium carrier concentration, the peak energy exhibits an S-shaped temperature dependence, where the W-shaped temperature dependence of linewidth disappears. Instead, the linewidth first narrows, then increases monotonically; at high carrier concentration, the S-shaped temperature dependence of peak energy disappears. In addition, with the increase of temperature, the linewidth increases monotonically.

In our case, luminescence characteristics of peak 1 correspond well to the situation of medium carrier concentration, while the luminescence characteristics of peak 2 and peak 3 correspond well to the situation of low carrier concentration. This result is consistent with our experimental condition. As shown in Fig. 1, a 325-nm He–Cd laser with a rather low excitation power of 0.32 mW is used to pump the sample. The excitation light first reaches green MQWs, then gradually attenuates before reaching the pre-wells. In this case, the carrier concentration in pre-wells (peak 3) should be low. In green MQWs, the carriers are mainly concentrated in the deep localized states with lower energy (peak 1). Therefore, the carrier concentration in peak 2 (shallow localized states of green MQWs) is also low. Finally, peaks 2 and 3 are in the low carrier concentration regime while peak 1 is in the medium regime.

The temperature dependence of the linewidth can be described by the following equation:[32]

$$\Gamma(T) = \Gamma_0 + \Gamma_{LA} \cdot T + \frac{\Gamma_{LO}}{\left(\exp\left(\frac{E_{LO}}{k_B \cdot T}\right) - 1\right)}, \tag{5}$$

where Γ_0 is the linewidth due to the inhomogeneous broadening caused by impurities and defects, Γ_{LA} is related to longitudinal-acoustic-phonon (LA-phonon) scattering, Γ_{LO} is related to longitudinal-optical-phonon (LO-phonon) scattering, and E_{LO} is the phonon energy determined by indium content (subscripts LA and LO denote the LA phonons and LO phonons, respectively). The data for the temperatures in the 175 K–300 K range are chosen for the fitting the results shown in Fig. 6. The values of Γ_0 for peaks 1–3 are 140.6, 80.6, and 36.1 meV, respectively. Both peak 1 and peak 2 originate from green InGaN/GaN MQWs and the larger values of Γ_0 in peak 1 and peak 2 are ascribed to their higher indium content. Sim-

ilarly, the smallest value of Γ_0 in peak 3 corresponds to the lowest indium content in pre-wells.

According to Vegard's law, the higher indium-containing InGaN/GaN MQWs correspond to a larger deformation potential energy and a stronger acoustic phonon–exciton interaction.[33,34] However, the Γ_{LA} values for peaks 1–3 are 0.01, 0.01, and 0.15 meV, respectively. In other words, the Γ_{LA} value for peak 3 is larger than those for peaks 1 and 2, indicating the presence of a stronger acoustic phonon–exciton interaction in the pre-wells with lower indium content. This suggests that the stress mainly appears in the pre-wells, rather than in the green InGaN/GaN MQWs with the higher indium content. This demonstrates that the pre-wells exert a significant stress blocking effect.

On the other hand, the LO-phonon is related to the degree of polarization in the nitride. However, the spontaneous polarization and piezoelectric polarization in InN are larger than those in GaN, and therefore, the indium content is the key factor affecting the LO-phonon interaction. The Γ_{LO} values for peaks 1 and 2 obtained by our analysis are quite different, suggesting that a strong polarization exists in the localized state of the green InGaN/GaN MQWs with high indium content.

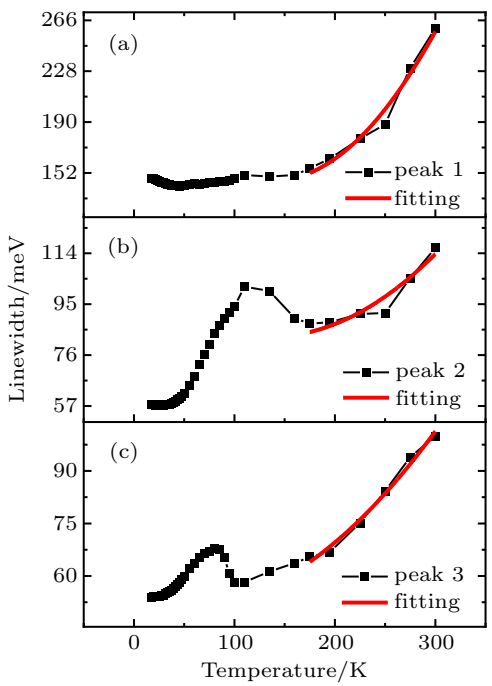

Fig. 6. Temperature-dependent linewidths of (a) peak 1, (b) peak 2, and (c) peak 3.

Table 4. Fitting results of temperature-dependent linewidth.

	Peak 1	Peak 2	Peak 3
Γ_0/meV	140.6	80.6	36.1
Γ_{LA}/(meV/K)	0.01	0.01	0.15
Γ_{LO}/meV	3384.0	910.9	623.8
E_{LO}/meV	89	89	90

To determine the IQE, the TRPL results are used to calculate the carrier lifetime. The TRPL intensity is analyzed by using a two-channel decay model and the results are shown in Fig. 7. The TRPL intensity is given by

$$I(t) = I_0 + A \cdot \exp\left(-\frac{t}{\tau_{\text{initial}}}\right) + B \cdot \exp\left(-\frac{t}{\tau_{\text{final}}}\right), \quad (6)$$

where τ is the carrier lifetime that can be decomposed into the initial stage of the decay time (τ_{initial}), and the final stage of the decay time (τ_{final}).[35]

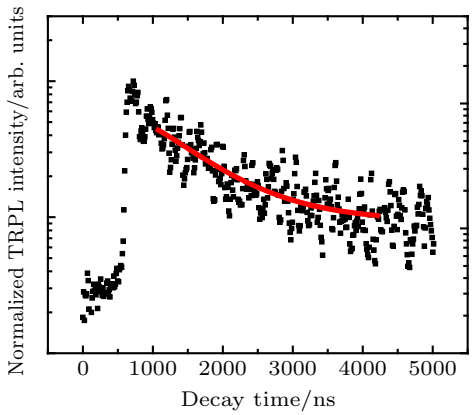

Fig. 7. Normalized TRPL intensity varying with decay time and fitted curve for green MQWs at 300 K.

Using the two-channel decay TRPL fitting model, we obtain τ_{initial} and τ_{final} to be 323.5 ns and 832.6 ns, respectively. Then, the non-radiative recombination carrier lifetime (τ_{nr}) and the radiative recombination carrier lifetime (τ_{r}) are obtained from the following equation:[36]

$$\tau_{\text{r}} = \frac{2 \cdot \tau_{\text{initial}} \cdot \tau_{\text{final}}}{\tau_{\text{final}} - \tau_{\text{initial}}}, \quad \tau_{\text{nr}} = 2 \cdot \tau_{\text{final}}, \quad (7)$$

and finally, from the IQE of the sample is obtained to be 61.1% from

$$\text{IQE} = \left(\frac{1+\tau_{\text{r}}}{\tau_{\text{nr}}}\right)^{-1}. \quad (8)$$

Thus, our sample can achieve high-efficiency green emission at room temperature,[37,38] which also indicates the beneficial effects of the pre-wells on the green InGaN/GaN MQWs.

4. Conclusions and perspectives

In this work, we investigated the mechanisms of luminescence in green InGaN/GaN MQWs and their pre-wells by TDPL in a temperature range of 17 K–300 K and by TRPL measurements at 300 K. The temperature dependence of the peak energy for green InGaN/GaN MQWs and for pre-wells both present an S-shaped variation, while the linewidth shows a complicated temperature dependence because the carriers hopping between localized states is influenced by the wide-range effect. By the fitting the solutions to the Varshini, Arrhenius, and linewidth equations, we investigated the properties of green InGaN/GaN MQWs and pre-wells through analyzing their localization effect, defect density, and phonon–exciton interaction. These results demonstrate the significant

stress blocking effect of pre-wells which is beneficial for the growth of green InGaN/GaN MQWs. Furthermore, our analysis of TRPL results verifies that the insertion of pre-wells is beneficial for enhancing the IQE of green InGaN/GaN MQWs. However, it is still necessary to perform a detailed comparison between the pre-wells and other films inserted before green InGaN/GaN MQWs in future work.

References

[1] Koike M, Shibata N, Kato H and Takahashi Y 2002 *IEEE J. Selec. Top. Quantum Electron.* **8** 271

[2] Zhang J Y, Cai L E, Zhang B P, Hu X L, Jiang F, Yu J Z and Wang Q M 2009 *Appl. Phys. Lett.* **95** 161110

[3] Strite S, Lin M E and Morko H 1993 *Thin Solid Films* **231** 197

[4] Weng G, Mei Y, Liu J, Hofmann W and Zhang B 2016 *Opt. Express* **24** 15546

[5] Queren D, Avramescu A, Bruederl G, Breidenassel A, Schillgalies M, Lutgen S and Strauss U 2009 *Appl. Phys. Lett.* **94** 689414

[6] Chang J Y, Chang Y A, Chen F M, Kuo Y T and Kuo Y K 2013 *IEEE Photon. Technol. Lett.* **25** 55

[7] Weng G E, Zhao W R, Chen S Q, Akiyama H, Li Z C, Liu J P and Zhang B P 2015 *Nanoscale Res. Lett.* **10** 1

[8] Jeong H, Jeong H J, Oh H M, Hong C H, Suh E K, Lerondel G and Jeong M S 2015 *Sci. Rep.* **5** 9373

[9] Tawfik W Z, Bae S J, Ryu S W, Jeong T and Lee J K 2014 *Opt. Mater.* **38** 131

[10] Yun Ji W L, Talha Erdem, Rui Chen, Swee Tiam Tan, Zi-Hui Zhang, Zhengang Ju, Xueliang Zhang, Handong Sun, Xiao Wei Sun, Yuji Zhao, Steven P. DenBaars, Shuji Nakamura and Hilmi Volkan Demir 2014 *Appl. Phys. Lett.* **104** 143506

[11] Pecharromán-Gallego R, Martin R W and Watson I M 2004 *J. Phys. D: Appl. Phys.* **37** 2954

[12] Rajabi K, Wei Y, Ding L, He J, Hua Z, Ji Q, Shen B, Yan T and Hu X 2015 *Superlattices & Microstructures* **80** 102

[13] Alam S, Sundaram S, Elouneg-Jamroz M, Li X, El Gmili Y, Robin I C, Voss P L, Salvestrini J P and Ougazzaden A 2017 *Superlattices & Microstructures* **104** 291

[14] Wang J X, Wang L, Zhao W, Zou X and Luo Y 2010 *Sci. China: Technol. Sci.* **53** 306

[15] Langer T, Jo?Nen H, Kruse A, Bremers H, Rossow U and Hangleiter A 2013 *Appl. Phys. Lett.* **103** 022108

[16] Wang L, Wang L, Yu J, Hao Z, Luo Y, Sun C, Han Y, Xiong B, Wang J and Li H 2018 *Acs Appl. Mater. & Interfaces* **11** 1228

[17] Cheng Y C, Lin E C, Wu C M, Yang C C, Yang J R, Rosenauer A, Ma K J, Shi S C, Chen L C and Pan C C 2004 *Appl. Phys. Lett.* **84** 2506

[18] Lai M H, Zheng Z W, Yu J, Ying L Y and Zhang B P 2016 *J. Korean Phys. Soc.* **68** 1291

[19] Kumar M S, Park J Y, Lee Y S, Chung S J, Hong C H and Suh E K 2007 *J. Phys. D: Appl. Phys.* **40** 5050

[20] Yang F, Zhang Y T, Han X, Li P C, Jiang J Y, Huang Z, Yin J Z, Zhao D G, Zhang B L and Du G T 2016 *Superlattices & Microstructures* **91** 259

[21] Wei T, Zhang L, Ji X, Wang J, Huo Z, Sun B, Hu Q, Wei X, Duan R and Zhao L 2014 *IEEE Photon. J.* **6** 1

[22] Zeng Y P, Liu W J, Wen G E, Zhao W R, Zuo H J, Yu J, Zhang J Y, Ying L Y and Zhang B P 2015 *Chin. Phys. Lett.* **32** 064207

[23] Huang Y, Duan X, Cui Y and Lieber C M 2002 *Nano Lett.* **2** 101

[24] Shmagin I K, Muth J F, Kolbas R M, Mack M P, Abare A C, Keller S, Coldren L A, Mishra U K and Denbaars S P 1997 *Appl. Phys. Lett.* **71** 1455

[25] Reshchikov M A and Morkoc H 2005 *J. Appl. Phys.* **97** 061301

[26] Ramaiah K S, Su Y K, Chang S J, Kerr B, Liu H P and Chen I G 2004 *Appl. Phys. Lett.* **84** 3307

[27] Liang M M, Weng G E, Zhang J Y, Cai X M, Xue Q L, Ying L Y and Zhang B P 2014 *Chin. Phys. B* **23** 054211

[28] Xing B, Cao W Y and Du W M 2010 *Chin. J. Lumin.* **6** 864

[29] Yu C X, L W, Z L Wang, Zhi B H, Yi L B, Chang Z S, Yan J H, Bing X, Jian W, and Hong T L 2017 *J. Appl. Phys.* **122** 135701

[30] Wang H, Ji Z, Qu S, Wang G, Jiang Y, Liu B, Xu X and Mino H 2012 *Opt. Express* **20** 3932

[31] Shan W, Little B D, Song J J, Feng Z C and Stall R 1996 *Appl. Phys. Lett.* **69** 3315

[32] Hammersley S, Watson-Parris D, Dawson P, Godfrey M J, Badcock T J, Kappers M J, McAleese C, Oliver R A and Humphreys C J 2012 *J. Appl. Phys.* **111** 083512

[33] Rahman M A and Islam M R 2014 *Developments in Renewable Energy Technology*

[34] Kim K, Lambrecht W R L and Segall B 1996 *Phys. Rev. B* **53** 16310

[35] Li Q, Wang S, Gong Z N, Yun F, Zhang Y and Ding W 2016 *Optik* **127** 1809

[36] Ebaid M, Kang J H, Lim S H, Ko S M, Cho Y H and Ryu S W 2014 *Acta Mater.* **65** 118

[37] Kawakami Y, Nishizuka K, Yamada D, Kaneta A, Funato M, Narukawa Y and Mukai T 2007 *Appl. Phys. Lett.* **90** 261912

[38] Murotani H, Shibuya K, Yoneda A, Hashiguchi Y, Miyoshi H, Kurai S, Okada N, Tadatomo K, Yano Y and Tabuchi T 2019 *Jpn. J. Appl. Phys.* **58**